

## Supporting information

### Defect-Induced Photogating Effect and its Modulation in Ultrathin Free-standing Bi<sub>2</sub>O<sub>2</sub>Se Nanosheets with Visible to Near- Infrared Photoresponse

Md Tarik Hossain<sup>1</sup>, Tadasha Jena<sup>2</sup>, Subhankar Debnath<sup>1</sup> and P. K. Giri<sup>1, 2\*</sup>

<sup>1</sup>Department of Physics, Indian Institute of Technology Guwahati, Guwahati -781039, India

<sup>2</sup>Centre for Nanotechnology, Indian Institute of Technology Guwahati, Guwahati 781039,  
India

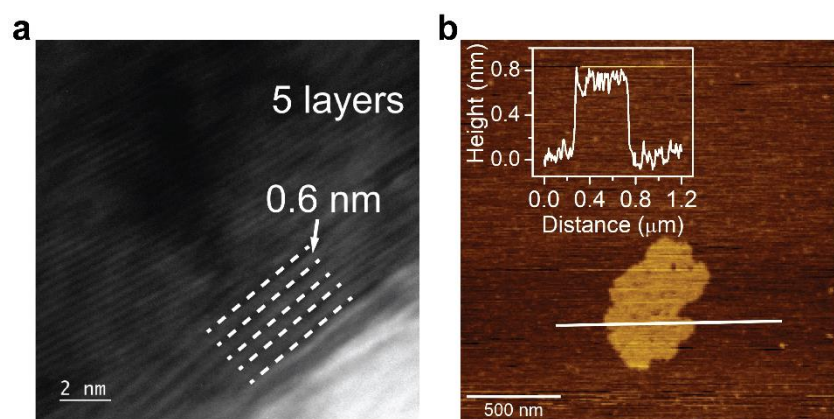


**Fig. S1:** (a) TEM image showing an edge of Bi<sub>2</sub>O<sub>2</sub>Se NS containing 5 layers (3 nm thickness). (b) AFM image of a single monolayer Bi<sub>2</sub>O<sub>2</sub>Se nanosheet. The inset shows the corresponding height profile of the monolayer Bi<sub>2</sub>O<sub>2</sub>Se.

\* Corresponding authors, email [giri@iitg.ac.in](mailto:giri@iitg.ac.in) (PKG).

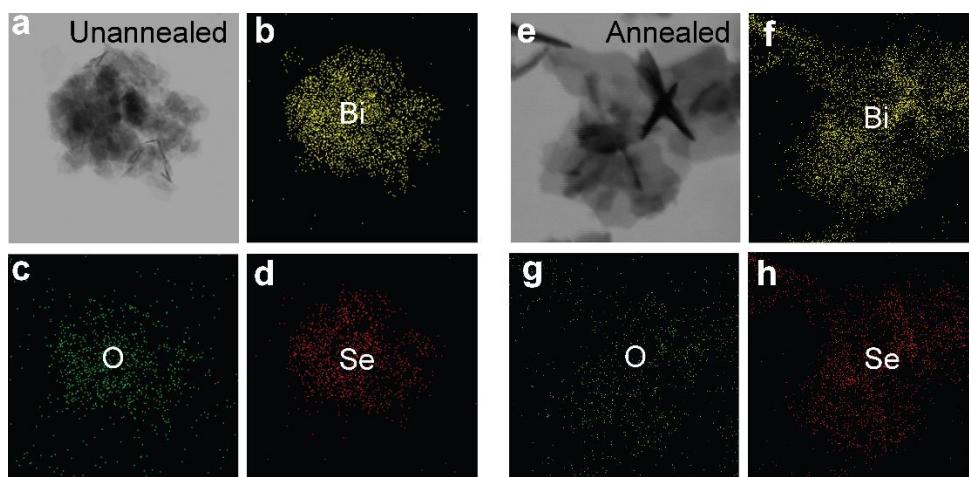


**Fig. S2:** (a) Bright-field TEM image of unannealed  $\text{Bi}_2\text{O}_2\text{Se}$  NS. (b-d) The corresponding STEM elemental mapping of Bi (yellow), O (green), Se (red). (e) TEM image of annealed NS, (f-h) the corresponding Bi, O, Se mapping.

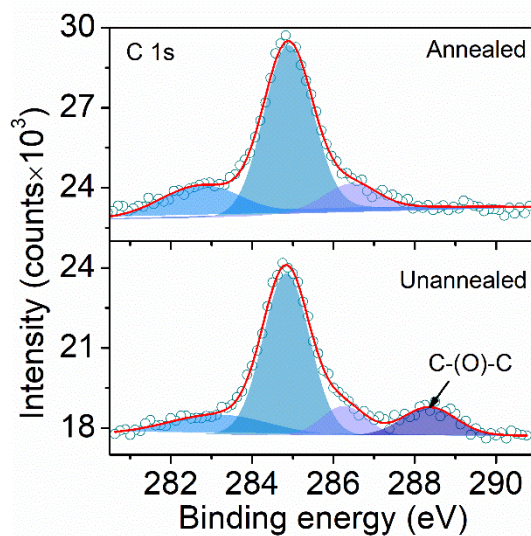


**Fig. S3:** Comparison of the XPS C 1s spectra of unannealed (lower panel) and annealed (upper panel)  $\text{Bi}_2\text{O}_2\text{Se}$  NSs.

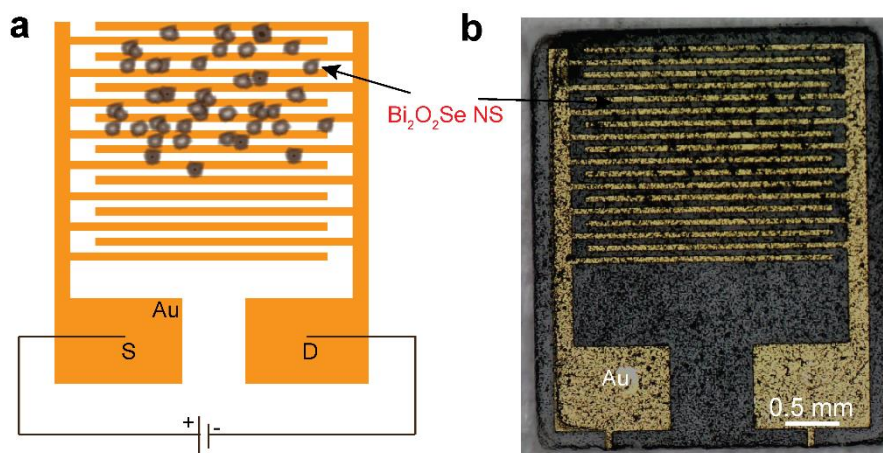


**Fig. S4:** (a) Schematic of the IDE pattern with  $\text{Bi}_2\text{O}_2\text{Se NS}$  (device) used for photoresponse measurement. (b) The corresponding digital photograph of a measured device.

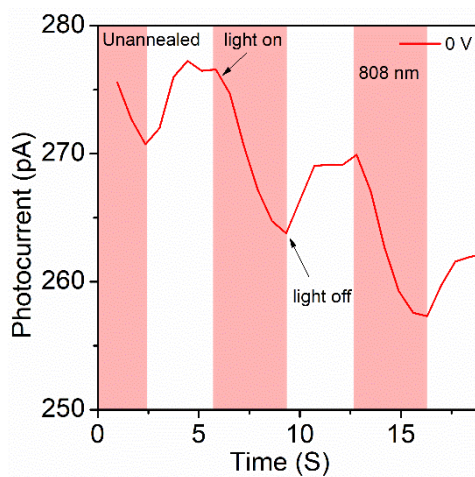


**Fig. S5:** Photocurrent with pulsed light (as a function of time) at 0V for unannealed  $\text{Bi}_2\text{O}_2\text{Se NS}$  showing the self-powered feature.

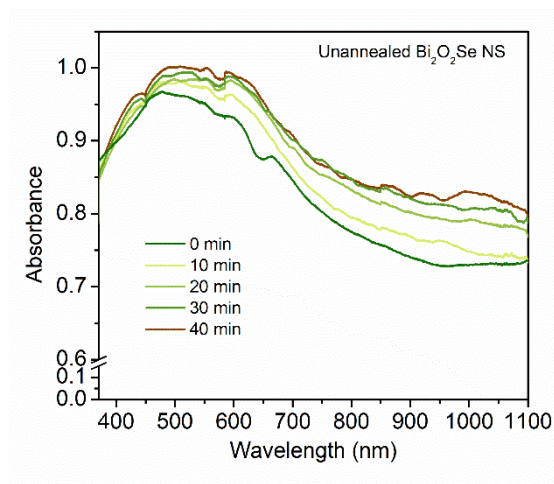


**Fig. S6:** Absorption spectra of unannealed Bi<sub>2</sub>O<sub>2</sub>Se NS after different durations of light exposure.

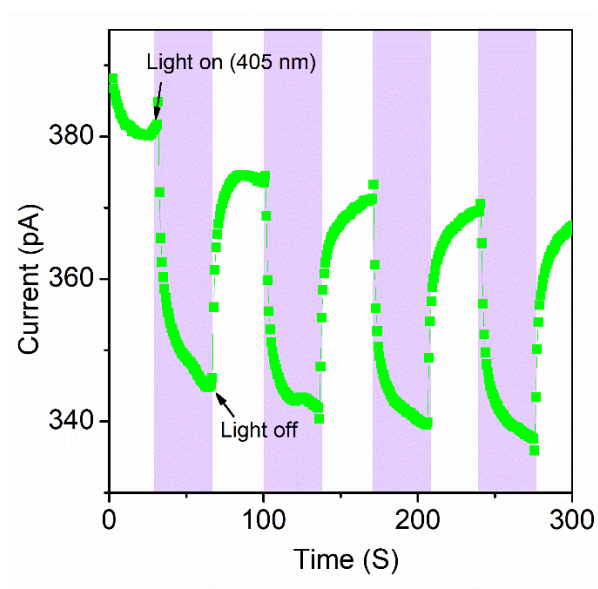


**Fig. S7:** Photocurrent response as a function of time for 405 nm excitation pulse, showing negative photoconductivity effect.

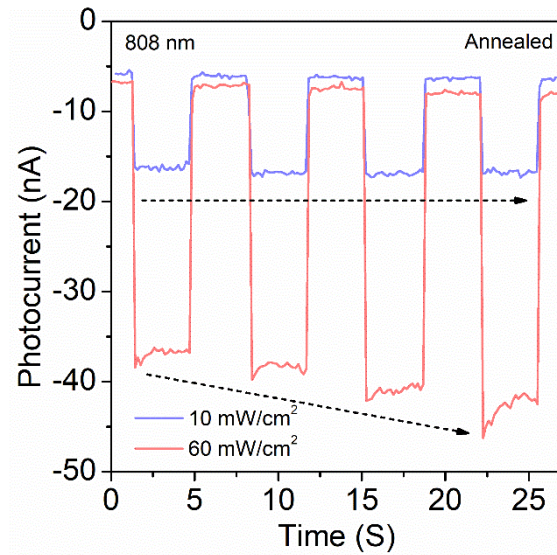


**Fig. S8:** Photocurrent as a function of time for annealed NS at two different intensities (laser) showing the bolometric effect at higher power.

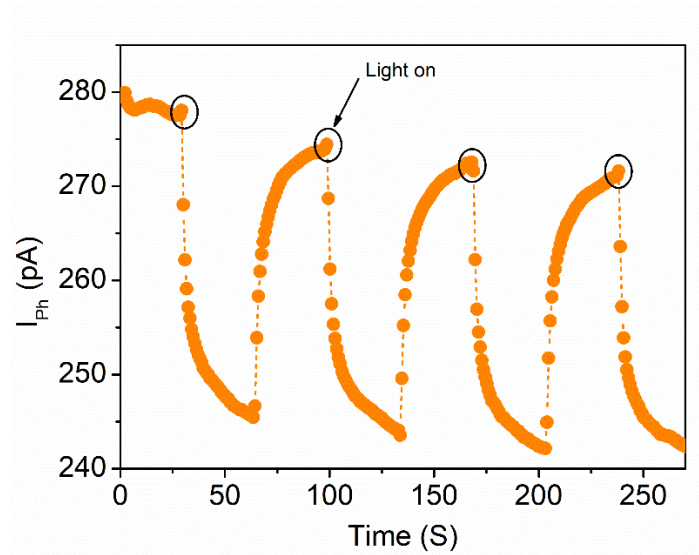


**Fig. S9:** Pulsed photocurrent under 808 nm excitation showing transition of positive PC (encircled) to negative PC at the time of turning on the light.

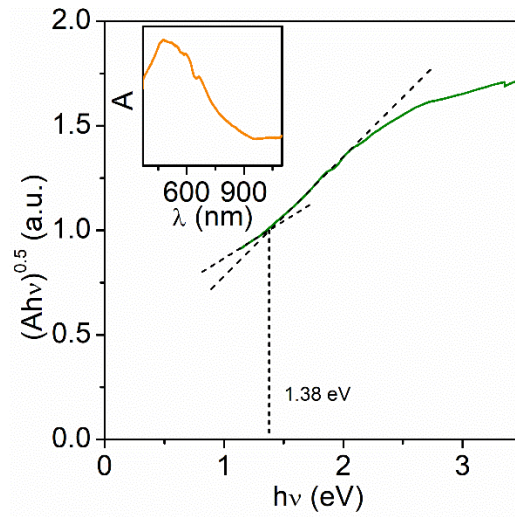


**Fig. S10:** Tauc plot indicating the band gap of 1.38 eV. The inset shows the corresponding absorption spectrum.

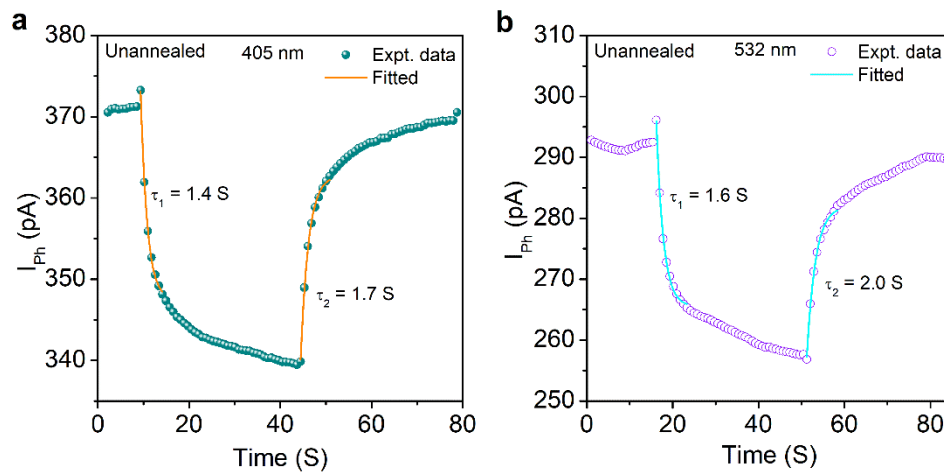


**Fig. S11:** Photocurrent response time (decay and rise) of unannealed Bi<sub>2</sub>O<sub>2</sub>Se photodetector under (a) 405 nm, (b) 532 nm pulsed lasers. The solid lines correspond the exponential fittings to initial decay/rise and the symbols are the experimental data.

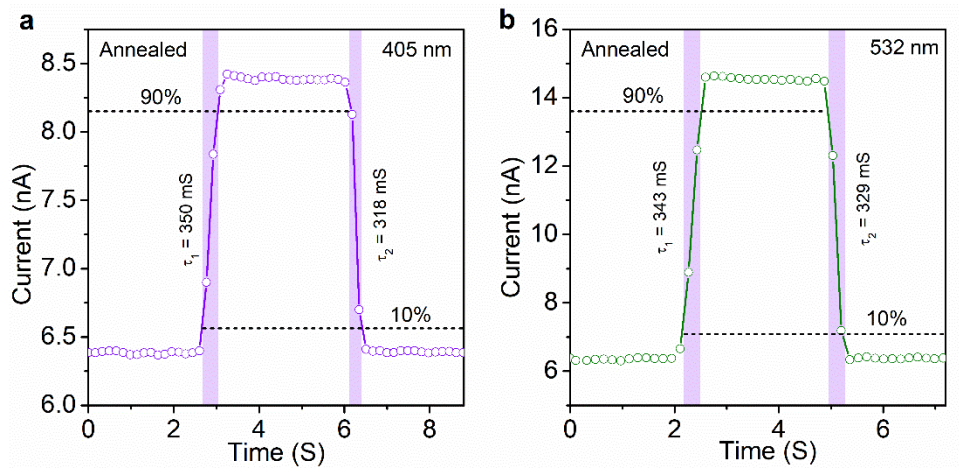


**Fig. S12:** Photocurrent response time (decay and rise) of annealed  $\text{Bi}_2\text{O}_2\text{Se}$  based photodetector under (a) 405 nm, and (b) 532 nm pulsed lasers.

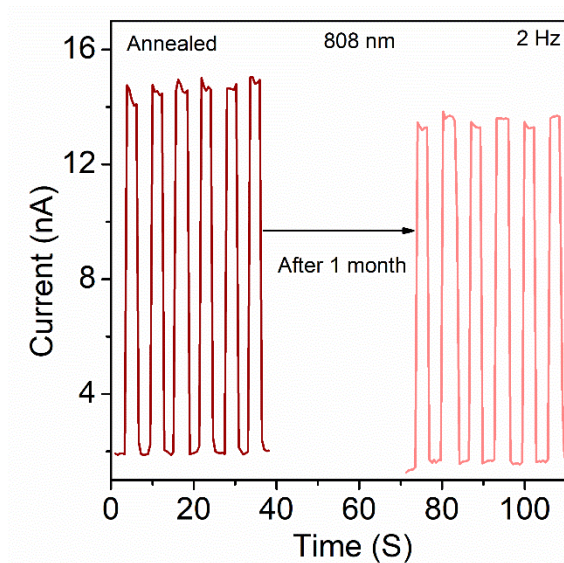


**Fig. S13:** Comparison of photocurrent response between freshly prepared and one-month old (storage in ambient condition) annealed  $\text{Bi}_2\text{O}_2\text{Se}$  photodetector showing good stability.

**Table S1:** XPS peak positions for different elements in unannealed and annealed NS.

<i>XPS peaks</i>		<i>Binding energy (eV)</i>	
		<i>Unannealed NS</i>	<i>Annealed NS</i>
Bi 4f	Bi 4f 7/2	158.1	153.2
	Bi 4f 5/2	163.4	163.5
O 1s	O 1s (I)	529.1	529.4
	O 1s (II)	531.0	531.6
	O 1s (III)	532.8	533.6
Se 3d	Se 3d 5/2	52.3	52.6
	Se 3d 3/2	53.1	53.4
C 1s	C 1s	284.8	284.8
	C-(O)-C	288.4	absent